A Critical Comparison of Three Methods for Time-Lapse Time-Shift Calculation

Lu Ji[1] · Colin MacBeth[2] · Marie-Daphne Mangriotis[2]

Abstract Time-shift, one of the most popular time-lapse seismic attributes, has been widely used in dynamic reservoir characterization by linking it with pressure and geomechanical changes. Therefore, it is important to select appropriate calculation methods according to different time-lapse seismic data quality and time-shift magnitude. To date, there have been various published works comparing different time-shift calculation methods and discussing their advantages and disadvantages. However, most of these comparisons are based only on synthetic tests or single field applications. As the quality of time-lapse seismic data and time-shift magnitude can vary in different fields, one method may not work consistently well for each case. In this paper, a critical comparison of three different time-shift calculation techniques (Hale's fast cross-correlation, Rickett's non-linear inversion, and Whitcombe's correlated leakage method) is provided. The three methods are applied to a set of synthetic data sets that are designed to account for various seismic noise and time-shift magnitudes. They are also applied to four real time-lapse seismic data sets from three North Sea fields. The calculated time-shift results are compared with the input (in synthetic tests) or the real observations from information such as seabed subsidence and compaction (in field applications). Both qualitative and quantitative comparisons are performed. At the end, each of the time-shift methods is evaluated based on different aspects, and the most appropriate method is suggested for each data scenario. All three time-shift methods are found to successfully measure time-shifts. However, Rickett's non-linear

✉ Lu Ji
  lj_uk17@hotmail.com

[1] China University of Petroleum - Beijing, Beijing 102249, China

[2] Edinburgh Time-Lapse Project, School of Energy, Geoscience, Infrastructure and Society, Heriot-Watt University, Edinburgh EH14 4AS, UK

inversion is the most outstanding method, as it gives smooth time-shifts with relatively good accuracy, and the derived time strains are more stable and interpretable.

Keywords Time-shift calculation · Time-lapse seismic · Methods comparison · Cross-correlation · Non-linear inversion

1 Introduction

Time-lapse seismic data are widely used in dynamic reservoir characterization and management, such as in mapping out bypassed/residual oil for new drilling opportunities (Koster et al. 2000), for displacement efficiency evaluation and waterfront detection to avoid the costly mistake of drilling new wells into swept zones (Kloosterman et al. 2003), to accurately separate the effect of pressure changes and saturation changes (Landrø 2001), for predicting geomechanical effects, and for monitoring well performance. Time-lapse time-shift (Δt) is one of the most popular time-lapse seismic attributes used in dynamic reservoir characterization. It represents the two-way travel-time (TWT) difference between time-lapse seismic surveys both inside and outside the reservoir. For example, during the development of a hydrocarbon field, pressure changes inside the reservoir will lead to changes in stress and strain fields of rock formations both inside and outside the reservoir (Hatchell and Bourne 2005), which will cause a certain degree of deformation (thickness change) as well as seismic velocity change in these formations. As a result, seismic waves propagating through them will have different travel time before and after production which can be measured from time-lapse seismic surveys, and these TWT differences are time-lapse time-shifts.

Theoretically, time-shifts can be measured very accurately in discrete, regularly sampled time-lapse seismic data, with the only limitation being the signal-to-noise ratio of the data. As a general concern, improper acquisition and processing can affect the time-shift measurements (Fehmers et al. 2007). In practice, the accuracy also depends on the measurement algorithms. Since the concept of time-lapse time-shift was introduced, a large number of measurement techniques have been published. However, there are inherent limitations within each method, and the accuracy of recovering various magnitudes of time-shifts from various qualities of time-lapse seismic data needs to be evaluated. Unsuitable calculation methods in some cases will produce unreliable results and can even introduce artificial noise, which will bias the interpretation (Kanu et al. 2016). Therefore, selecting a proper time-shift calculation method for different application scenarios is a significant challenge to be tackled at the very beginning.

In this paper, first, a variety of time-shift calculation methods published so far are reviewed, along with their inherent shortcomings. Based on this review, three typical methods—Hale's fast cross-correlation (DHFCC) (Hale 2007), Rickett's non-linear inversion (NLI) (Rickett et al. 2007), and Whitcombe's correlated leakage method (CLM) (Whitcombe et al. 2010)—are programmed and applied to both synthetic and real time-lapse seismic data sets. Finally, the calculated time-shifts and derived time strains are compared to give insights into the selection of the most suitable method for different types of data sets.

2 Time-Shift Calculation Methods

2.1 Cross-Correlation-Based Techniques

Over the past two decades, there have been a variety of methods developed for the measurement of time-lapse time-shifts, among which the most common is cross-correlation. This technique is a measure of the similarity between two data sets as a function of the lag, and its function is often normalized as (Gubbins 2004)

$$\text{NCC}_j = \frac{\sum_i a_i b_{i+j}}{\sqrt{\sum_i a_i^2 \sum_i b_i^2}}, \tag{1}$$

where NCC is the cross-correlation coefficient, a and b denote the two seismic data sets, i represents each node in seismic traces, and j is the lag.

It should be noted that $\left| \text{NCC}_j \right| \leq 1$, and that NCC_j is equal to 1 only when the two series are perfectly identical (Gubbins 2004). By finding the maximum cross-correlation coefficient, the time-shift is returned in proportion to the lag. Hall et al. (2002) developed a stable warping approach which calculates time-shifts along horizons. Later, sliding windows are preferred in cross-correlation-based methods to capture the spatial variability of time-shifts, for example the fast cross-correlation method by Rickett et al. (2006) and the three-dimensional cross-correlation technique by Hale (2007). However, these two methods differ in the type of sliding window selected, in that, unlike the boxcar window in Rickett et al. (2006), Hale (2007) chooses the Gaussian window, so that three-dimensional 'blobs' of data are cross-correlated. Moreover, instead of just recovering for time-shift, Dave Hale's method calculates three displacement components (vertical time-shifts, inline lateral shifts, and cross-line lateral shifts) simultaneously.

In Hale's fast cross-correlation method (DHFCC), a cyclical search is performed for local cross-correlation, whereby a sequence of correlations and shifts along each spatial dimension are applied to the seismic cubes (Hale 2007). Therefore, at a given iteration step, the shifts found in the previous step are applied to one of the cubes before the next correlation. A new set of shifts is then calculated—first vertically, and then in the horizontal direction. This process is repeated until all shifts become negligible, and it has been found that four iterations are enough for time-shift calculation (Hale 2009). In addition, to improve the spatial resolution, whitening and smoothing filters are applied to both seismic vintages before correlation.

Although the cross-correlation-based techniques have been commonly used, they are not without problems. Their windowed nature means that there are inherent limitations of resolution and accuracy. Increasing the length of the sliding window will give smoother images as this process stabilizes the time-shift estimation, however, at the cost of reducing the resolution. In contrast, a short window can provide more details in the time-shift profile, but this faces the risk of miscorrelation of events if one of the events being correlated is outside the window, thus losing the value of the event in future time-strain derivation, as it is too noisy. For these reasons, a good window parameter needs to be determined before performing the calculation, and this
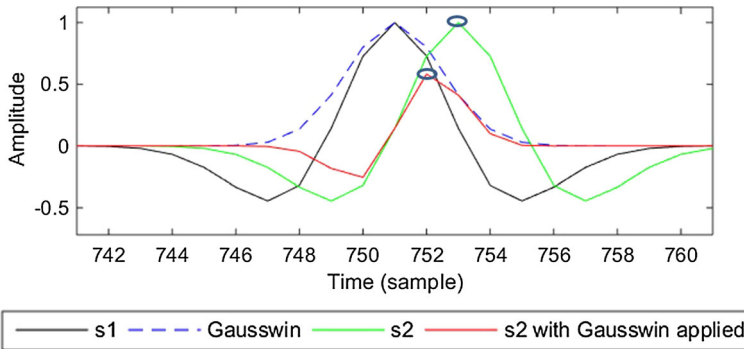
Fig. 1 An illustration of the bias caused by a Gaussian window. After the Gaussian taper is applied, the peak event in s2 is shifted towards s1, and this will make the recovered time-shift smaller than the true value

is usually done through trial and error. Another issue is with the tapers used in some techniques (e.g., Gaussian tapers in DHFCC). Although they help to stabilize the time-shift estimation and reduce spectral leakage when used properly (Gubbins 2004), they may bias predictions if the length of each taper is too short (Hodgson 2009). Figure 1 illustrates the bias caused by a Gaussian taper, where s2 is a time-shifted version of s1. After the Gaussian taper is applied, the location of the peak in s2 is shifted towards s1, and this will reduce the time-shift value to be recovered in cross-correlation.

2.2 Non-Cross-Correlation-Based Techniques

Non-cross-correlation techniques have also been developed in recent years, which include inversion-based approaches such as the non-rigid matching developed by Nickel et al. (2001) and the non-linear inversion method by Rickett et al. (2007) which gives smooth time-shift results, and Taylor-expansion-based approaches such as the method described in Hatchell et al. (2003) which performs derivations on the original seismic traces and the correlated leakage method by Whitcombe et al. (2010) which works better than Hatchell's, as it avoids the derivation step to increase calculation accuracy. In addition, some interesting techniques have been developed to recover time-shift in the pre-stack domain (Fuck et al. 2007; Lie 2011), or by going to the time-time domain (Zabihi Naeini 2013). Instead of direct time-shift calculation, Williamson et al. (2007) propose a non-linear inversion method to predict velocity perturbations, which is further modified by Grandi et al. (2009) to invert for time strains.

The non-linear inversion (NLI) method (Rickett et al. 2007) aims to find the time-shift that, once applied, will minimize the misfit between base and monitor seismic volumes. The least-squares objective function is formed as

$$E = |d - f(m)|^2 + \alpha \, |\nabla_x m|^2 + \beta \, \left|\nabla_y m\right|^2 + \gamma \, \left|\nabla_t^2 m\right|^2, \qquad (2)$$

where m contains the time-shift volume, $f(m)$ contains the time-shifted monitor, and d contains the baseline. ∇x, ∇y, and ∇t^2 are imposed for spatial constraints and vertical constraint, respectively. The three weights (α, β, γ) control the relative weighting of the three smoothing constraints. The objective function is solved via linearization of the current model, solving of the resulting linear problem, and consequent updating of this model, via the descent-based Gauss–Newton algorithm (Hodgson 2009). Before performing the NLI method, three smoothing weights need to be chosen, usually through trial and error until they give the most satisfactory result from an interpretation perspective.

The correlated leakage method (CLM) devised by Whitcombe et al. (2010) finds an innovative way to calculate the time-shifts. In this approach, time-shifts are measured from the gradient of a line fitted to a cross-plot, in which the y-axis contains the amplitude difference between the baseline and monitor (Eq. 3), and the x-axis contains the amplitude difference between the baseline and monitor average and a time-shifted version of this average (Eq. 4) (Whitcombe et al. 2010). The Taylor expansion functions for the x and y axes are expressed as

$$Y = M - B = f(t+a) - f(t) \approx \left[f(t) + af'(t) \right] - f(t) = af'(t), \quad (3)$$

$$
\begin{aligned}
X &= \frac{\left[(B+M)_{i+1} - (B+M)_i \right]}{2} \\
&= \frac{[f(t+\Delta t) + f(t+\Delta t + a)] - [f(t) + f(t+a)]}{2} \\
&\approx \frac{\left\{ \left[f(t) + \Delta t f'(t) + f(t+a) + \Delta t f'(t+a) \right] - [f(t) + f(t+a)] \right\}}{2} \\
&= \frac{\Delta t f'(t) + \Delta t f'(t+a)}{2} \approx \frac{\left\{ \Delta t f'(t) + \left[\Delta t f'(t) + a \Delta t f''(t) \right] \right\}}{2} \\
&\approx \Delta t f'(t),
\end{aligned}
\quad (4)
$$

where Δt is a user-defined time-shift, $f''(t)$ is the second derivative of $f(t)$, and a is the time-shift to be estimated.

The least-squares approach is used for finding the best gradient of each line fitted to the cross-plot, and this method is expanded to the three-dimensional domain by cross-plots of three-dimensional patches of data within a sliding window. Compared with another approach, by Hatchell and Bourne (2005), which also uses the Taylor expansion, the correlated leakage method works better, as it avoids performing derivations on the original seismic traces, and instead uses seismic traces directly for the calculation. Similar to the approximations made in Taylor expansion calculation, this method works well in small time-shift scenarios, and should be carefully applied if large time-shifts are expected. A simple one-dimensional comparison of the three selected time-shift methods (NLI, CLM, and cross-correlation) was performed by MacBeth et al. (2016) (Fig. 2). The results show general consistency among the three methods, but also some clear differences.

In this paper, a comprehensive comparison has been conducted to study the applicability of different methodologies (DHFCC, NLI, and CLM) in recovering time-shifts
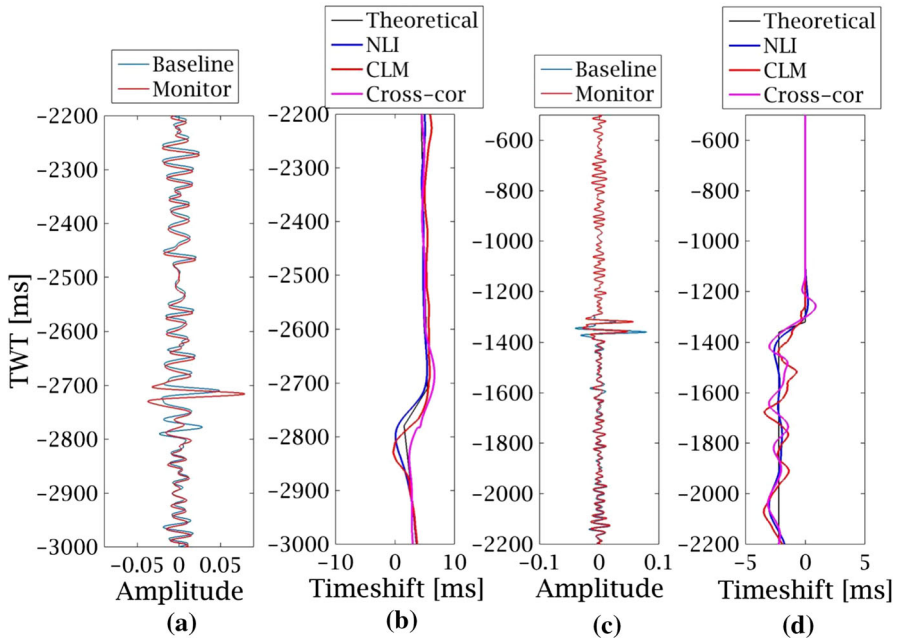
Fig. 2 Baseline and monitor traces of two synthetic one-dimensional cases (**a**, **c**) with measurements of time-shifts from three different methods (**b**, **d**)

from various seismic data sets, where a series of synthetic tests have been carried out, followed by field data applications.

3 Comparison of Methods with Application to Synthetic Data

3.1 Description of Synthetic Tests

To prepare for the synthetic data sets, a two-dimensional section was extracted from the 1989 Ekofisk survey as the baseline seismic (Fig. 3c), and the synthetic monitor was then created (Fig. 3d) by applying an already known, smoothly time-spatial-varying time-shift function to the base. This synthetic time-shift had a maximum magnitude of 8 ms, and was designed to mimic the distribution of that around a heavily compacted reservoir, with positive and negative values indicating slowdown (dilation) and speedup (compaction), respectively (Fig. 3a). Figure 3b shows the input time strain, which is the first-order derivative of the time-shift (Landrø and Janssen 2002; Landrø and Stammeijer 2004; Hatchell and Bourne 2005; Rickett et al. 2007).

3.2 Results of the Idealized Synthetic Time-Shift Tests

Figure 4 shows the results of the time-shifts calculated using DHFCC, CLM, and NLI, respectively, and the derived time strains. To ensure an unbiased comparison, the two
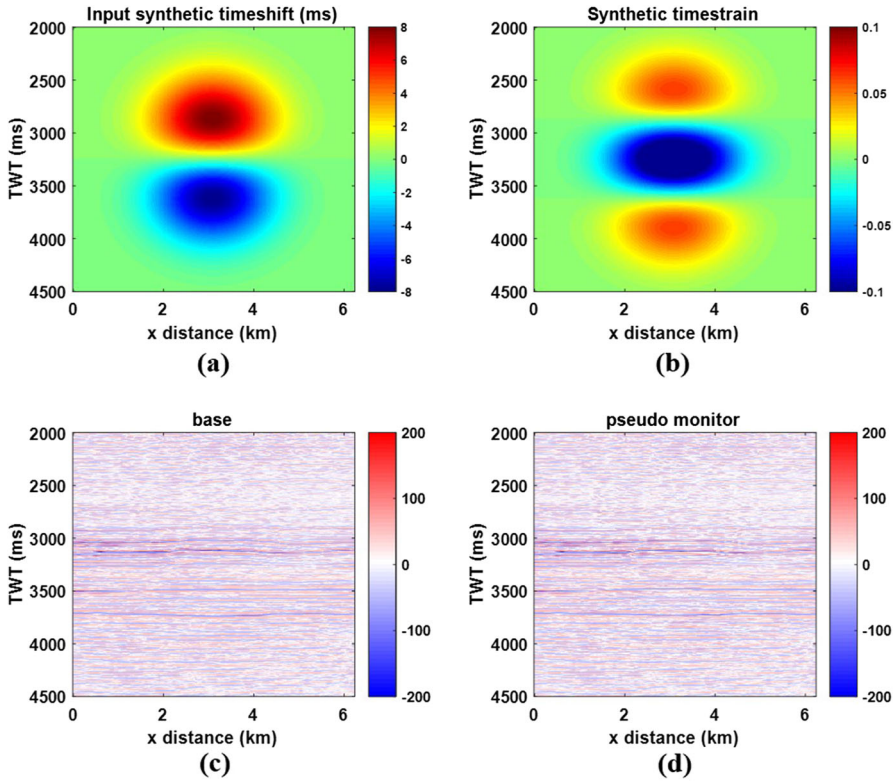
Fig. 3 a The input synthetic time-shift profile for creating the pseudo monitor survey. **b** The synthetic time strain derived from the input time-shift. **c** The base seismic extracted from the 1989 Ekofisk seismic survey. **d** The pseudo monitor after applying the input synthetic time-shift to the base seismic

window-based methods, DHFCC and CLM, were performed using the same size of sliding window. It is noted that the CLM method does not have a smoothing filter initially implemented; therefore, a Gaussian smoothing was applied in order to stabilize the final result. All three methods managed to recover the distribution pattern and time-shift magnitude very close to the input. When moving on to compare the derived time strains, the disparities become more obvious. Apart from the inherent noise caused by the derivation process, it can still be very clearly seen that the CLM result fails to recover the sharp change at the overburden/reservoir and reservoir/under-burden interfaces (Fig. 4d), while NLI gives the best results (Fig. 4f): by taking the difference between the estimated results and the inputs, a clearer qualitative comparison is obtained between the synthetic and estimated time-shift and time strain (Fig. 5).

To quantify the calculation error for each method, the normalized root-mean-square deviation (NRMSD) was calculated for each result as

$$\text{NRMSD} = \frac{\sqrt{\frac{1}{N} \sum_{i=1}^{N} (a_i - b_i)^2}}{\max(a) - \min(a)}, \tag{5}$$
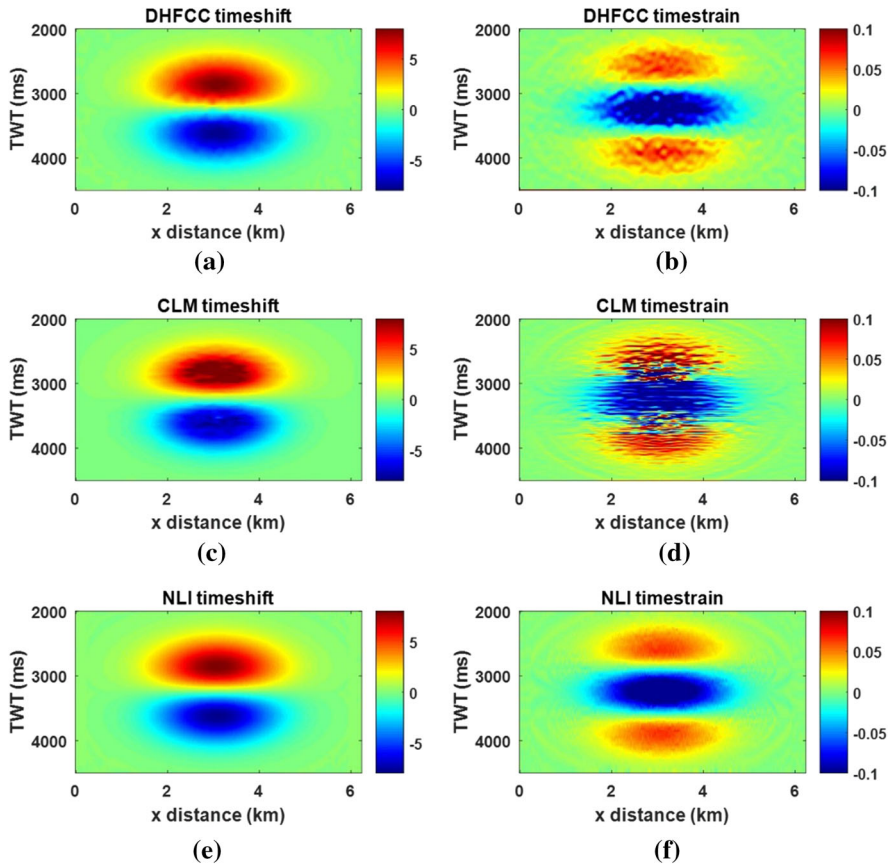
Fig. 4 a Time-shift calculated from DHFCC method, and **b** derived time strain. **c** Time-shift calculated from the CLM, and **d** derived time strain. **e** Time-shift calculated from NLI method, and **f** derived time strain

where a is the synthetic input, b is the calculation result, i denotes each sample, and N is the number of samples.

The results show that the higher the value of NRMSD, the lower the degree of matching between the two parameters under comparison; the NRMSD values for each method are displayed in Table 1. Clearly, the NLI method recovers the most accurate time-shift and time strain, which is best matched with the synthetic inputs, and the DHFCC results rank just below this. The residual variance in the CLM results is the highest of the three methods, especially for the time-strain estimation. This synthetic test shows that for even the best scenario with smoothly varying synthetic shifts and no noise or reflectivity changes between baseline and monitor, post-calculation smoothing is still required for the CLM result to approach the accuracy of the NLI result.
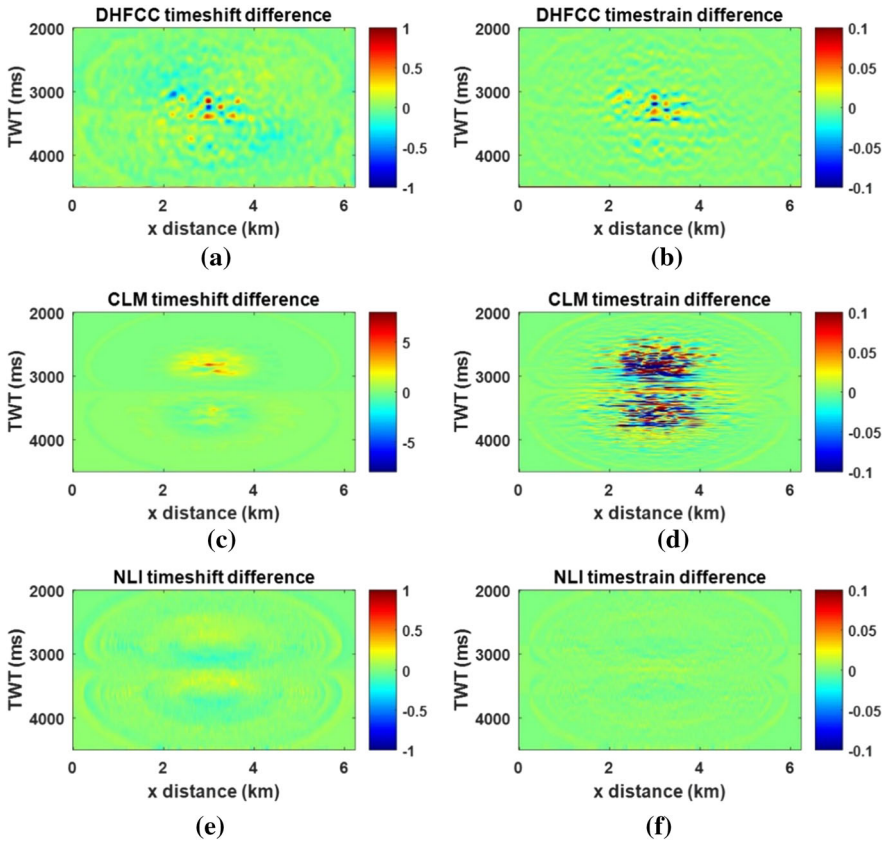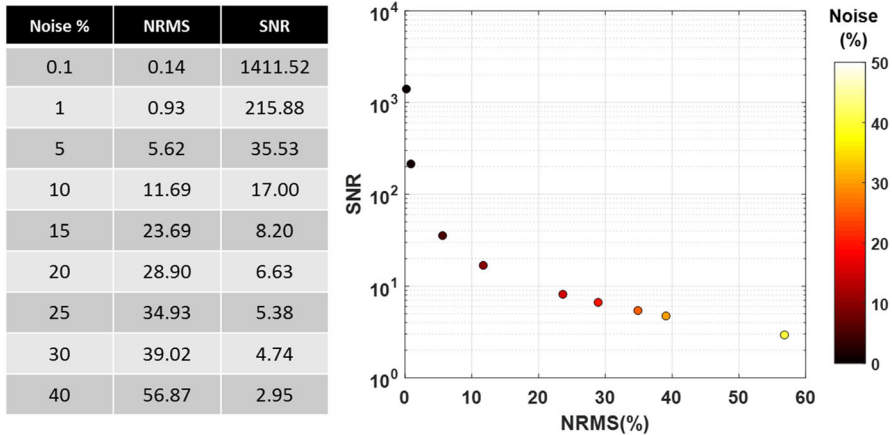
Fig. 5 Difference between synthetic time-shifts and estimated time-shifts using the DHFCC, CLM, and NLI, respectively

Table 1 The normalized root-mean-square deviation (NRMSD) of time-shift and time-strain results from all three methods compared with input synthetic time-shift and time-strain

Normalized root-mean-square deviation (NRMSD)

	DHFCC (%)	CLM (%)	NLI (%)
Time-shift	0.34	1.89	0.26
Time-strain	8.06	16.88	1.11

3.3 Noise Tests

The synthetic test above is an idealized scenario, which contains no additional noise; however, in the real world this situation never exists, as seismic data are always accompanied by noise. To facilitate these tests, different levels of random noise were applied to the previous synthetic data sets. It is important to note that random noise is only one source of noise within seismic data; other forms of noise also exist, but these are

Noise %	NRMS	SNR
0.1	0.14	1411.52
1	0.93	215.88
5	5.62	35.53
10	11.69	17.00
15	23.69	8.20
20	28.90	6.63
25	34.93	5.38
30	39.02	4.74
40	56.87	2.95

Fig. 6 Relationship among noise level, NRMS, and SNR for synthetic test

not a concern in the present paper. Here the imposed noise is in a range between 0 and 40% so that it favours the seismic repeatability close to the real data (e.g., NRMS is usually under 40% for North Sea fields).

Seismic repeatability can be calculated by the ratio of the root-mean-square of amplitude difference divided by the average RMS amplitude of the original surveys (Behrens et al. 2001) as

$$\text{NRMS} = \frac{2\sqrt{\sum (A - B)^2}}{\sqrt{A^2} + \sqrt{B^2}}, \tag{6}$$

where A and B are the two seismic volumes to be compared. The range of values of this particular metric is between zero for perfectly matched data and 2 for uncorrelated data.

The signal-to-noise ratio (SNR) between the two surveys can also be estimated from the NRMS (Behrens et al. 2001) as

$$\text{SNR} = \sqrt{2 - \text{NRMS}^2}/\text{NRMS}. \tag{7}$$

The range of values for the SNR is zero to infinity, and provides a comparison with the synthetic baseline and monitor before and after adding a different noise level. Figure 6 shows the calculated NRMS and SNR for different levels of random noise inserted in this synthetic test. The NRMS values in scenarios where noise levels vary between 5 and 20% are very close to some North Sea examples with large time-shifts.

As shown in Fig. 7, the NRMSD of both the CLM and NLI results increases with the increased noise level in the seismic data. When the noise level is less than 20%, the time-shift calculation errors from NLI and DHFCC are quite similar, and NLI is even better than DHFCC in recovering a good time-strain profile. However, when the noise level is higher than the 20% threshold, the behaviour of the two methods is reversed. Clearly, the DHFCC method does a very good job in dealing with very noisy data. To
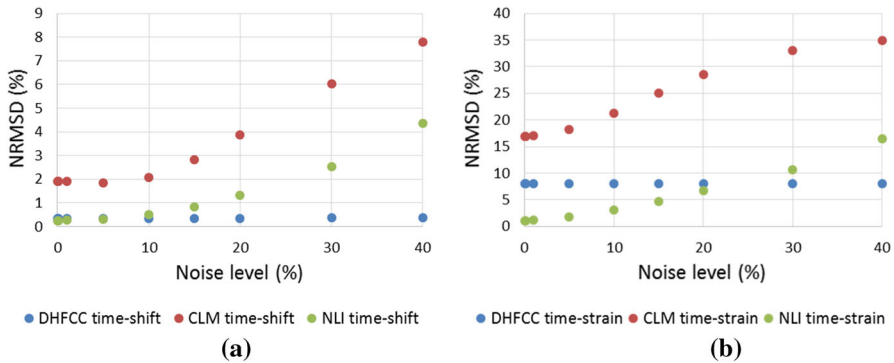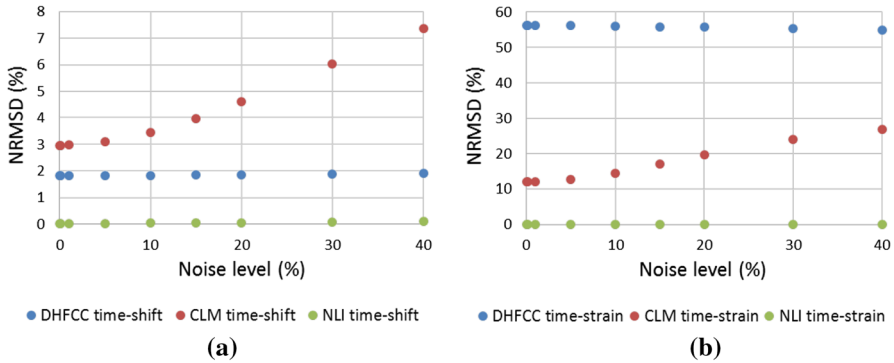
Fig. 7 The normalized root-mean-square deviation (NRMSD) of the calculated time-shift and time-strain results for seismic data with different noise levels, using the three methods

overcome the weakness of the NLI method in noisy data sets, we may need to apply a higher weight of smoothness constraints in the objective function, but this should be done in an appropriate way, as over-smoothing may bias the results.

3.4 Small Time-Shift Tests

In reality, the magnitude of observed time-shifts varies quite substantially depending on field production and recovery mechanisms, reservoir thickness, depth, and elapsed period, ranging from as small as 0.2 ms to as large as 20 ms or greater (MacBeth et al. 2019). The following synthetic tests are designed to account for small time-shift scenarios with various levels of background noise. Similarly to the previous work, a smoothly varying time-shift is created, but with a maximum magnitude of 1 ms, then input into the base data together with noise functions to create a set of monitors. After time-shift calculations were completed using the three methods, the results were compared with input time-shift data, as shown in Fig. 8. Compared with the results from previous large time-shift scenarios (Fig. 7), it can be seen that the NLI results are more stable in small time-shift scenarios, even when the noise level is high, and the CLM results are fairly close, apart from a small improvement in time-strain results. However, the DH technique does not appear to work very well for small time-shift scenarios, especially for subsequent time-strain derivation. The reason for this is that the smoothing process in the DH method has over-smoothed the time-shift signal, and has seen the real time-shift signal as noise, as both are in the same range.

It should be notice that, although it may seem to be straightforward, random noise is unrealistic. In reality, different noise models should be applied according to the overburden noise of the field (Wong 2017). Moreover, the noise test is the best-case scenario; only time-shift is included, without any reflectivity changes and no displacements in the lateral dimensions, which is not true for a real case. Next, a feasibility study is conducted to show how each method performs when applied to real seismic data sets in the North Sea.

Fig. 8 Cross-plots of normalized root-mean-square deviation (NRMSD) against noise level for the three time-shift measurement approaches; all data come from small time-shift tests

4 Comparison of Methods with Application to Field Data

In this section, the three time-shift measurement techniques are applied to four North Sea data sets from three different fields. Calculated time-shift results for each field will be compared laterally and will also be compared with published results, if they are available.

4.1 Application to the Ekofisk Field: Highly Compacting Reservoir

The first field for application is the Ekofisk field, which is situated in the south-western part of the Norwegian North Sea (Fig. 9a) with a water depth of about 72 m. The reservoir has an elongated anticlinal structure, with the long axis in the north–south direction, and the thickness of the overlying sediments is 2840 m at the crest (Sulak and Danielsen 1989). The reservoir consists of two fine-grained very-high-porosity and low-matrix-permeability limestone formations—the Danian Age Ekofisk formation and the Maastrichtian Age Tor formation—which are separated by a thin and impermeable tight zone (Fig. 9b). Since it was brought onstream in 1971, massive compaction has occurred due to reservoir production, which caused a 2.5 m subsidence at the seabed between 1973 and 1985 (Kvendseth 1988). Because of the water weakening of the formation chalk, reservoir compaction was not stopped, and full-field water injection was begun in 1987.

A seismic monitoring programme has been established at Ekofisk, with marine streamer time-lapse seismic surveys that were acquired over the field in 1989, 1999, 2003, 2006, and 2008. The NRMS values of seismic repeatability calculated using the Kragh and Christie (2002) equation range from 25 to 175, with an average of 80. In 2010, the Ekofisk life-of-field seismic project (referred to as LoFS) was installed, aiming to frequently acquire time-lapse seismic data of very high repeatability. The LoFS project has since been delivering outstanding seismic repeatability (NRMS of 3–5%), with clean, well-resolvable time-lapse signals and low residual time-lapse
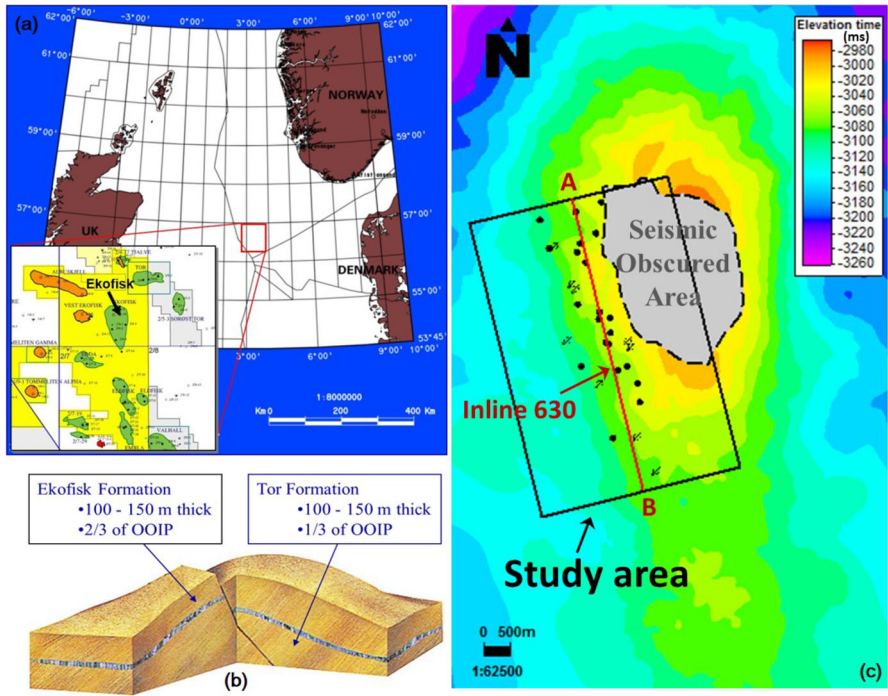
Fig. 9 **a** The location of the Ekofisk field (Tolstukhin et al. 2012). **b** A general illustration of the formation composition of the reservoir: above is the Ekofisk formation, below is the Tor formation, and they are separated by a thin impermeable zone. **c** Time map at the top reservoir: the grey-coloured area is the seismic obscured area caused by a gas cap. The study area is in the south-western part of this field, as illustrated by the black rectangle, and the red line inside shows the location of the cross-section which is used in the following analysis

noise (Buizard et al. 2013). Compaction-induced geomechanical changes in the overburden have resulted in time-lapse time-shifts as large as 20 ms (Folstad 2010).

For comparison of the methods, time-shifts are calculated from one set of towed streamer surveys (in 1989 and 2003) and one set of LoFS surveys (LoFS1 and LoFS2) for the area outlined in the black rectangle as shown in Fig. 9c. Through trial-and-error tests, a search window of 15 samples (60 ms) in the vertical axis and 12 traces (150 m) by 12 traces (150 m) in the x and y axes is used in the DHFCC and CLM calculations.

As shown in Fig. 10, the time-shift magnitude between the two towed streamer surveys is up to 10 ms; this is comparable to published values (Folstad 2010). The three time-shift maps are extracted at the top reservoir to represent the cumulative time-shift throughout the overburden interval. The blank area that appears in every map is caused by a gas cloud which obscured seismic signals. By plotting using the same colour bar each time, the similarity in time-shift distribution can be clearly seen, with a large positive time-shift in active production areas. However, a certain number of disparities in magnitude and distribution are also visible, for example in the two areas in the south of the time-shift maps (Fig. 10). Negative time-shifts are observed in these areas on both the CLM and NLI maps, but not on the DHFCC map. There are no
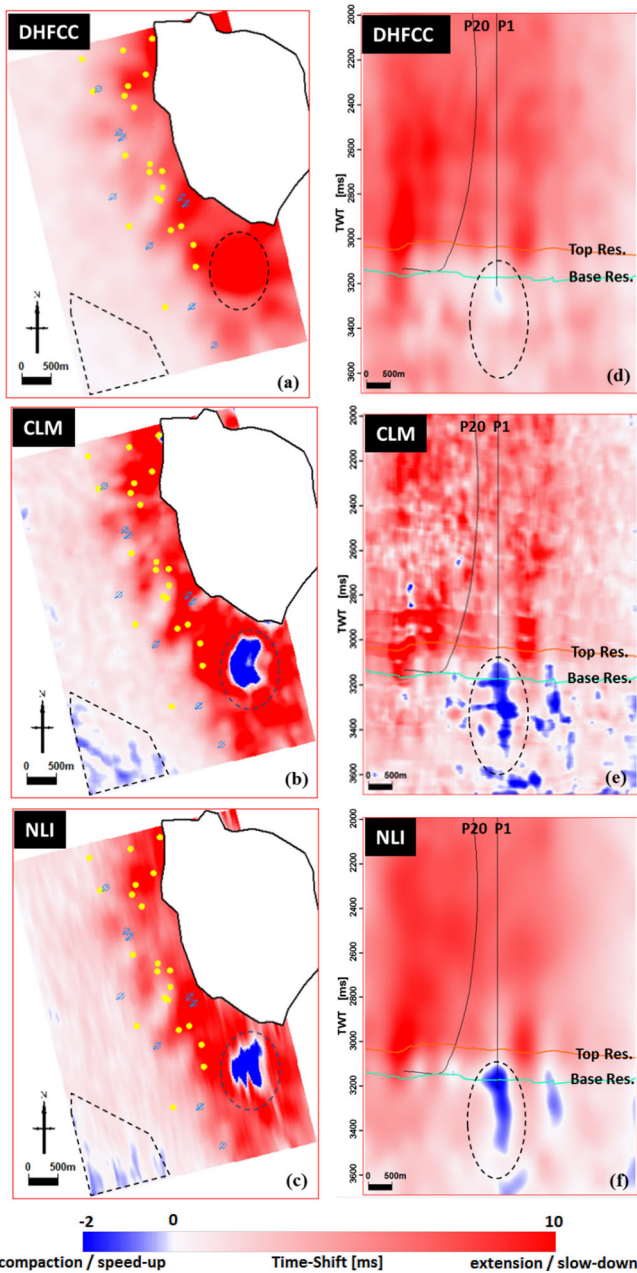
Fig. 10 Ekofisk time-shift results calculated by DHFCC, CLM, and NLI between 1989 and 2003 seismic data. Calculation errors are indicated by dashed lines; **a–c** are time-shift maps at the top reservoir, and **d–f** are time-shift sections of inline 630, as indicated by the red line AB in Fig. 9c
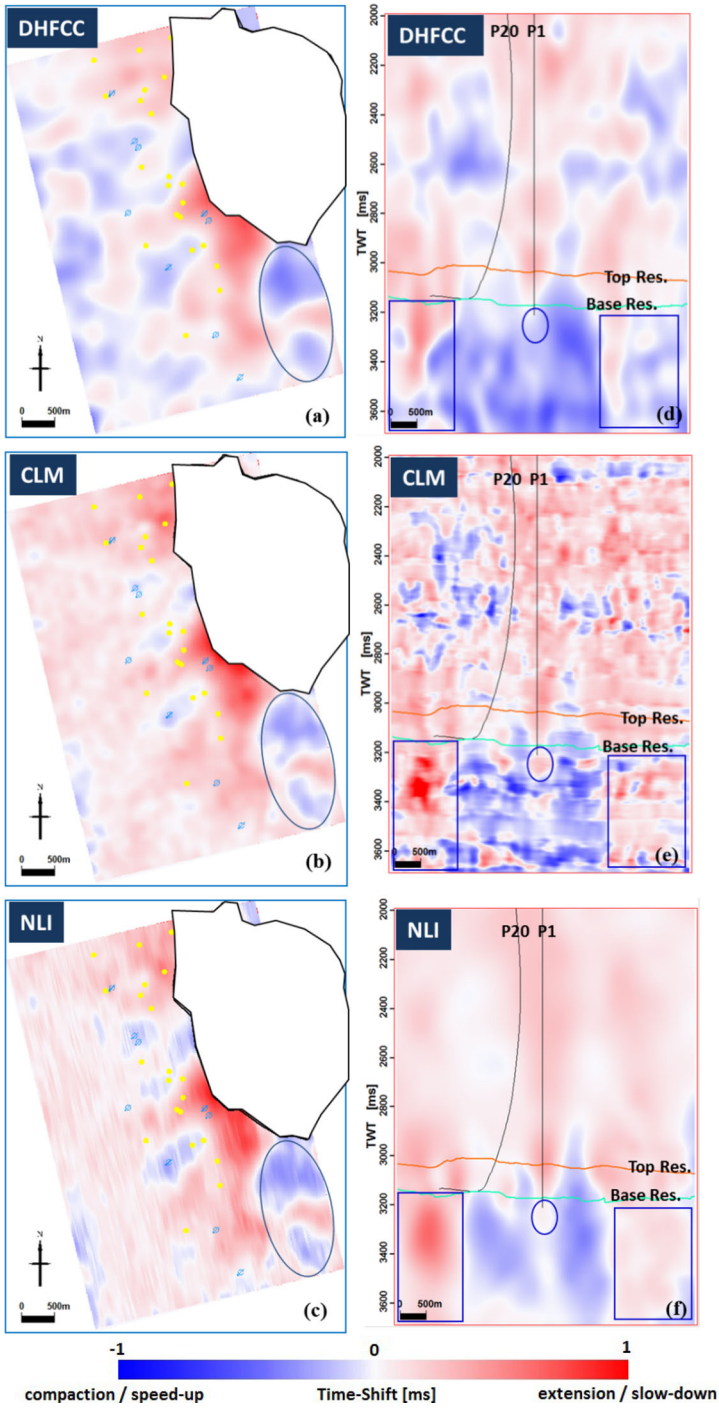
Fig. 11 Ekofisk time-shifts between LoFS1 and LoFS2 calculated by DHFCC (**a**, **d**), CLM (**b**, **e**), and NLI (**c**, **f**)
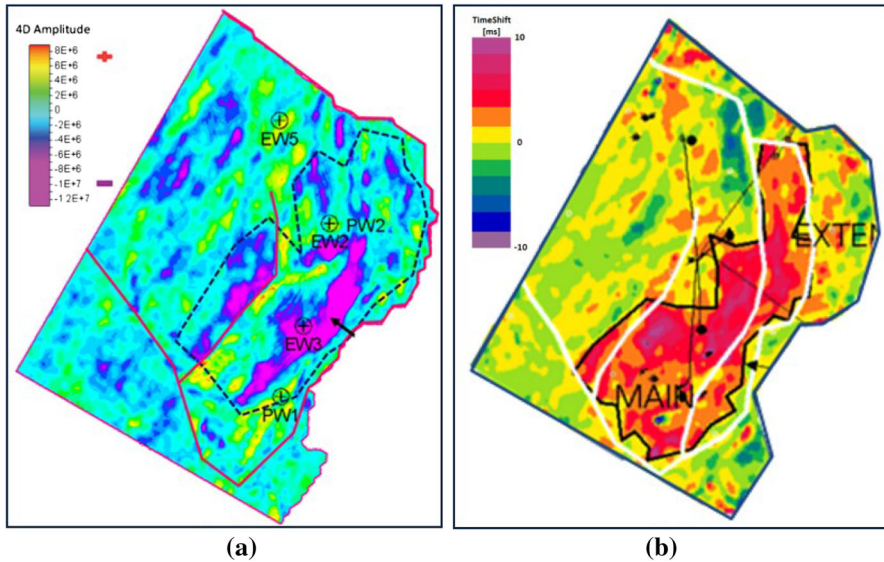
Fig. 12 a Time-lapse amplitude change across the reservoir (HajNasser 2012). **b** Time-shift map (Fletcher 2004). Extension pattern corresponds very well with field depletion pattern

wells in areas where results are not comparable, so the disparate time-shift distribution can hardly be genuine unless it is due to strong geomechanical changes. Examination of seismic sections in those areas reveals that these are calculation errors due to seismic noise and an inappropriate interpolation process. As mentioned earlier, the smoothing procedure in DHFCC is very efficient in suppressing noise for moderately repeated seismic surveys during large time-shift calculations.

Time-shift sections provide another perspective (Fig. 10). They are extracted from inline 630, which is in an intensive producing area. The orange horizon refers to the top reservoir and the blue horizon to the base reservoir. Time-shifts can be seen in all sections, which increase continuously through the overburden, and decrease inside the reservoir. In contrast to the small compaction signal in the upper reservoir around well P1, a stronger negative time-shift signal is picked up in both the CLM and NLI results. The strong reduction in time-shift is reflective of the greater compaction that occurred in the lower Ekofisk and Tor formations than in the top Ekofisk during production. This signal is weakened in the DHFCC result due to the tapering process, as mentioned earlier. A noise burst is found in the CLM result, especially in the under-burden interval.

As the two LoFS data sets were recorded 6 months apart, the estimated time-shift magnitude is relatively small, only around 1 ms. Again, time-shift maps were extracted at the top reservoir (Fig. 11); all three methods successfully brought out extension signals in the central producing area and confirmed each other at the southeast corner. However, the DH method did not suppress noise very well in the west area. The time-shift sections in Fig. 11 demonstrate roughly the same patterns. However, the extension signals picked up by CLM and NLI in both the left and right corners were attenuated by the DHFCC method, and in addition, the slowdown signal around P1 just
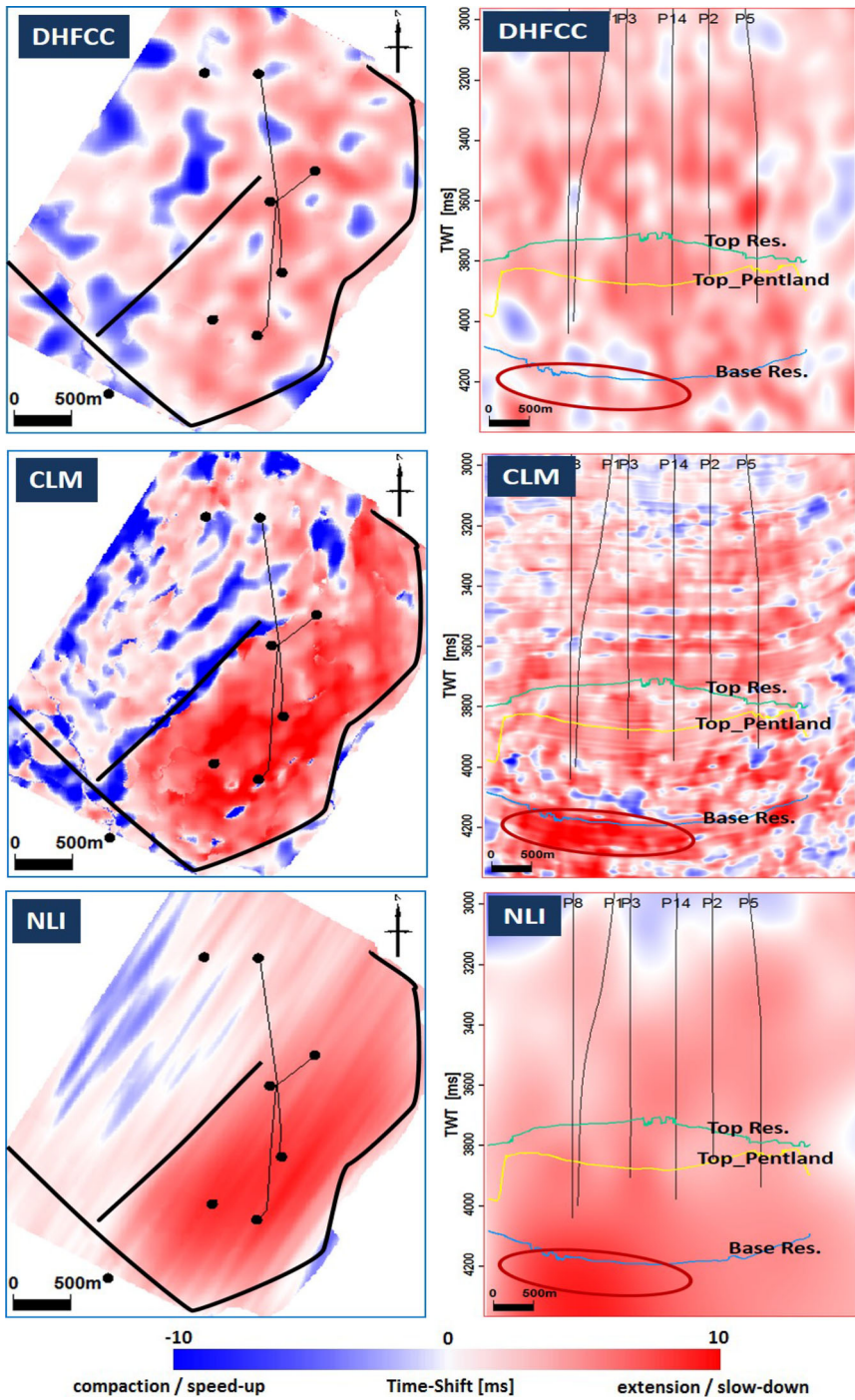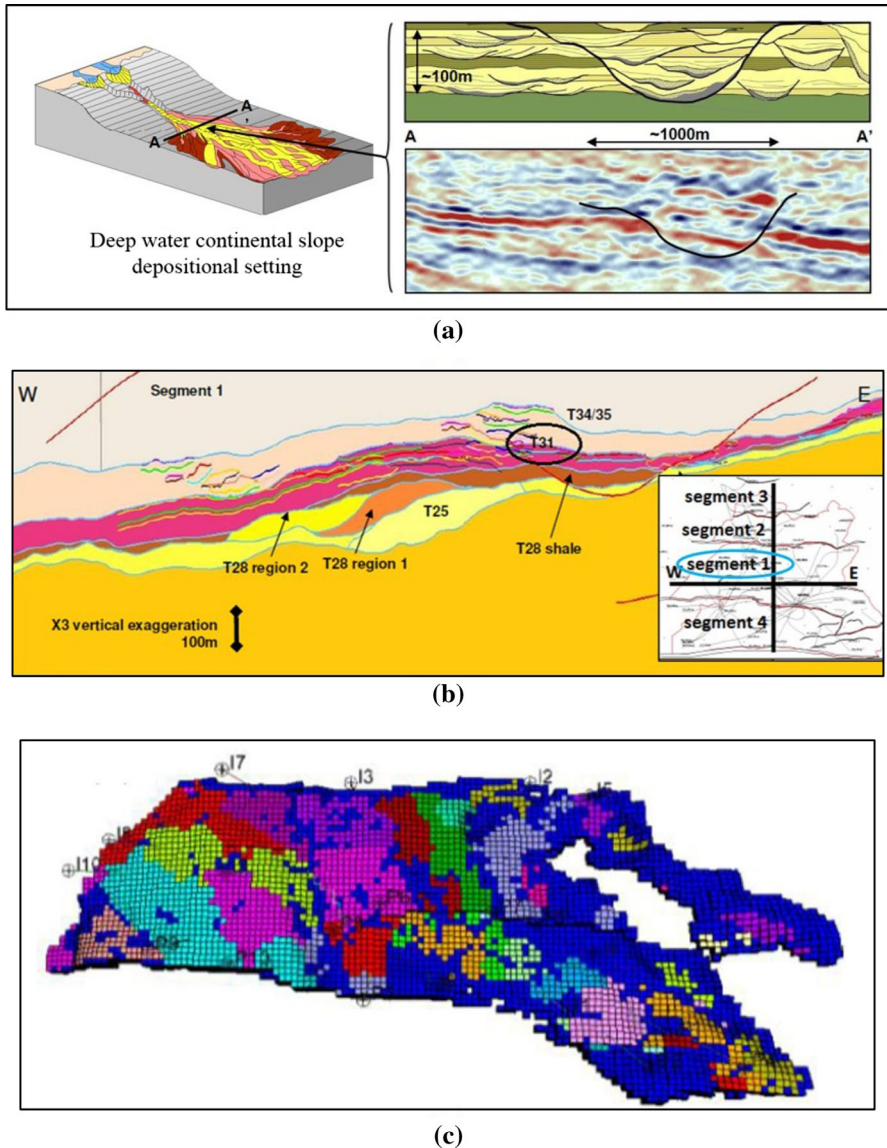
Fig. 13 Erskine time-shifts between 1989 and 2001 seismic data calculated by the three methods

(a)

(b)

(c)

Fig. 14 General geological information regarding the Schiehallion reservoir: **a** depositional environment and channelized structure of the sediments (Martin and Macdonald 2010); **b** geological cross-section (west to east) in Schiehallion segment 1 (Martin and Macdonald 2010); **c** the geological model of the Schiehallion reservoir in segment 1. These geobodies control the connectivity and fluid flow in the reservoir (Falahat 2012)

below the base reservoir was lost in the DH result. Noise is very well suppressed in the NLI result, while the CLM result seems to have the best resolution, as its distribution pattern reflects the geology to some degree.
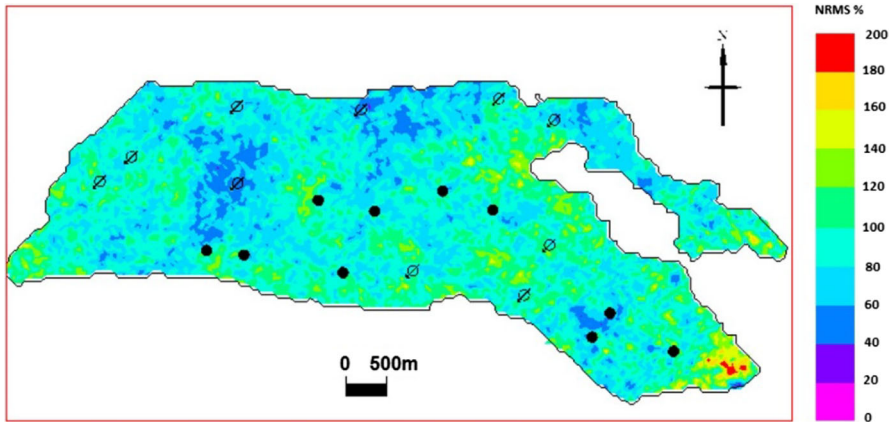
Fig. 15 Seismic repeatability (NRMS) in the overburden (calculated using the method proposed by Kragh and Christie 2002)
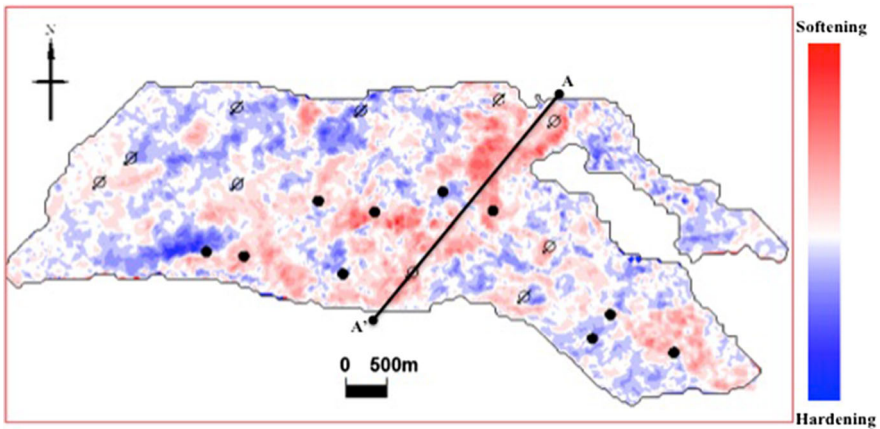
Fig. 16 Time-lapse map of the sum of negative amplitude between the top and base reservoir (between years 1998 and 2002)

4.2 Application to the Erskine Field: HPHT Gas Condensate Reservoir

The Erskine field is a high-temperature (340°F) and high-pressure (14,000 psi) (HPHT) gas condensate field which is located on the western margin of the East Central Graben (HajNasser 2012). The main reservoirs in this field are the Pentland, Erskine, and Heather formations, all of which were deposited during the Jurassic age. Massive pressure depletion occurred during the production period, which caused strong geomechanical changes. Time-lapse seismic surveys available in this field are the 1989 pre-production survey and the 2001 monitor seismic survey. The time-lapse amplitude map from HajNasser (2012) shows strong negative amplitude change concentrated around the producers in the eastern part, which matches the time-shift distribution reported by Fletcher (2004) (Fig. 12).
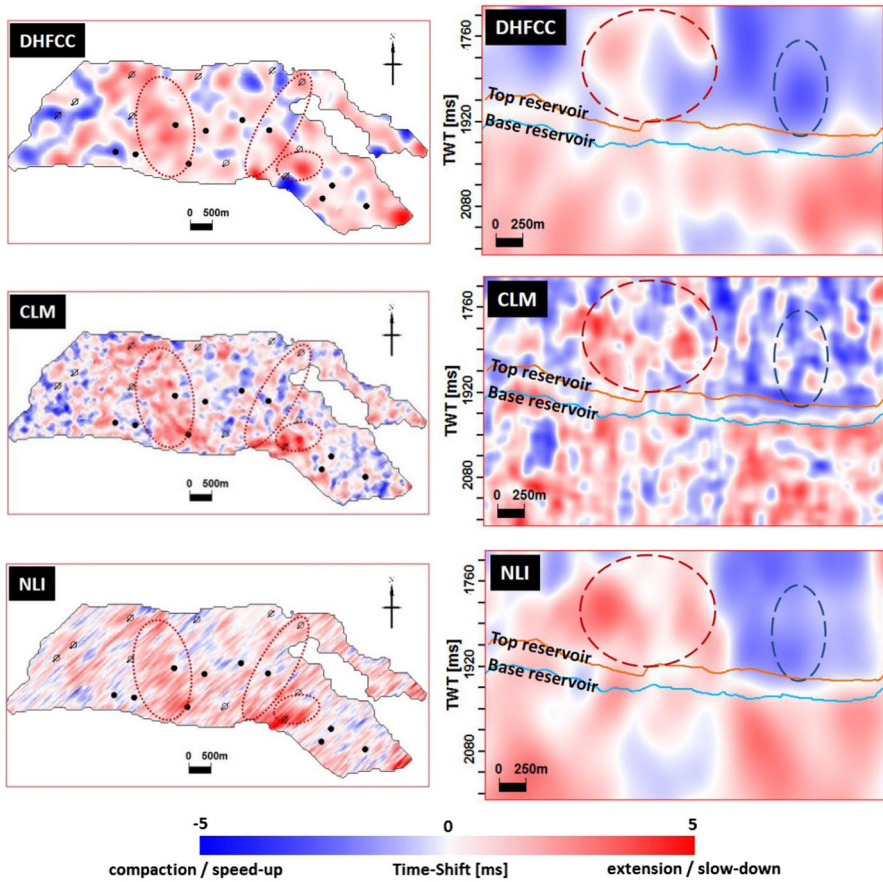
Fig. 17 Schiehallion time-shifts between 1996 and 2002 calculated by three methods

Figure 13 shows the time-shift results calculated by the DHFCC, CLM, and NLI techniques; as suggested in HajNasser (2012), a calculating window of size st9sx11sy11 (9 samples in vertical direction with a sample interval of 4 ms, and 11 samples in lateral direction with a sample interval of 12.5 m) was applied in the DHFCC and CLM. Time-shift maps were extracted at the base reservoir, with the main faults and producing wells plotted together. Compared with Fletcher's time-shift map in Fig. 11b, the present time-shift estimations match very well in terms of magnitude and distribution pattern. Both the CLM and NLI results clearly recover the positive time-shift distribution in the eastern area caused by the shale activation issue, while this character is attenuated by DHFCC. Moreover, the distribution of the CLM result corresponds quite well with the fault location, as it breaks along these faults, especially in the centre.

Among the three time-shift sections, the CLM has the best resolution, as it matches the deposition character of formations in this field. The NLI result is too smooth to reflect those features. Nevertheless, it is good to see that both pick up the same strong
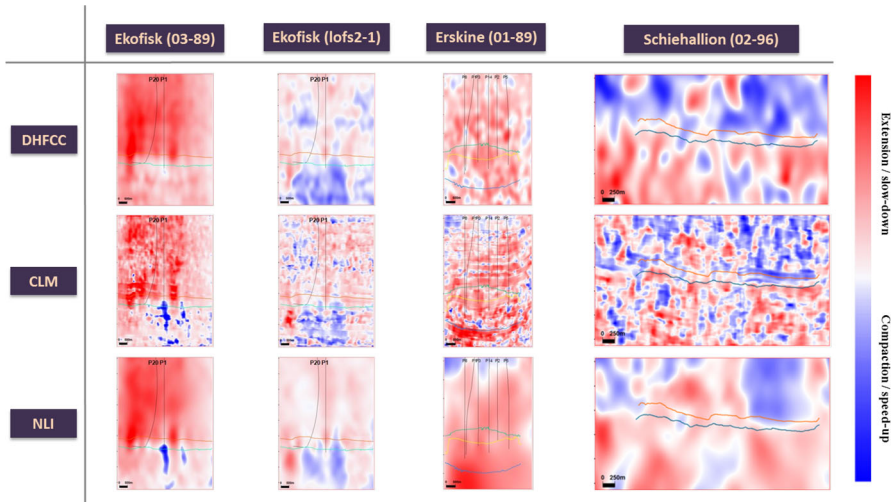
Fig. 18 Time-shift method comparison: section view of time-shift results from DHFCC, CLM, and NLI for four North Sea data sets
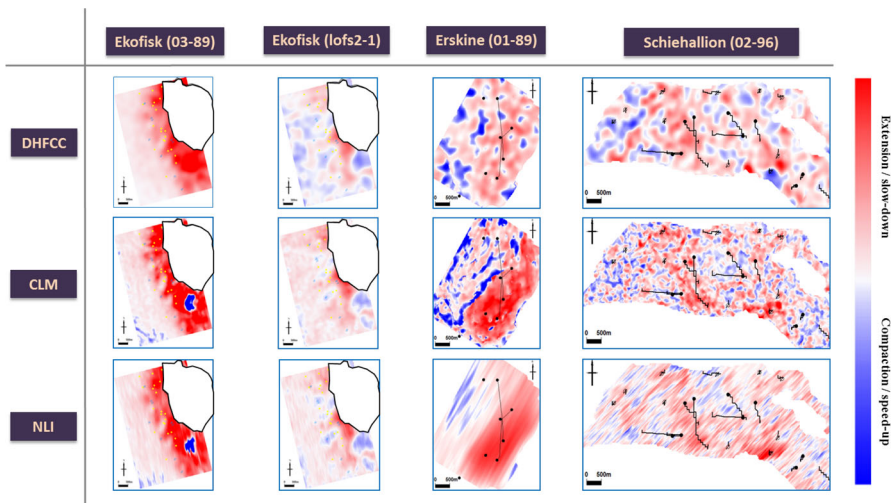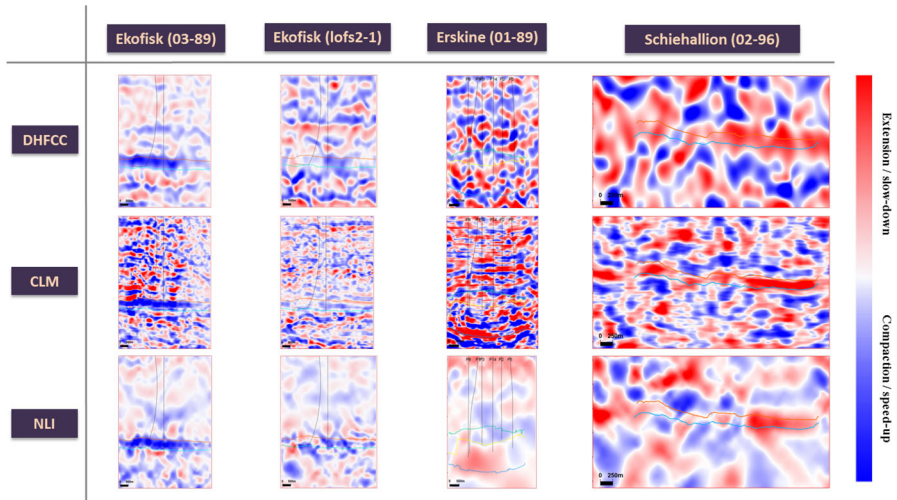

Fig. 19 Time-shift method comparison: map view of time-shift results from DHFCC, CLM, and NLI for four North Sea data sets

under-burden time-shifts on the left side, which may correspond to a combined effect of both geomechanical changes and production.

4.3 Application to the Schiehallion Field: Thin and Multiple-Stacked Reservoir

The final field for application is the Schiehallion field, which is situated on the United Kingdom continental shelf about 200 km to the west of the Shetland Islands and lies at

Fig. 20 Time-shift method comparison: section view of time-strain results derived from DHFCC, CLM, and NLI for four North Sea data sets

a water depth of about 450 m (Martin and Macdonald 2010). Deposited in a deepwater continental slope environment (Fig. 14a), the reservoir of the Schiehallion field comprises a complex Lower Tertiary sequence of amalgamated turbidite channel sands, which generally run from south-east to north-west, as shown in Fig. 14b (Martin and Macdonald 2010). A series of east–west-trending normal faults segregate the field and divide the reservoir into five distinct segments, with limited or no lateral communication (Falahat 2012). Because of the character of this field, a single segment (segment 1) is selected for this study. The reservoir quality of this field varies in character from poor-quality thinly interbedded sands and shale to high-quality massive sands with high porosity and permeability. Figure 14c shows the distribution of seismically recoverable geobodies that reveals the strong reservoir heterogeneity.

Multiple vintages of time-lapse seismic data have been shot in this field, among which the 1996 (pre-production) and 2002 (4 years after production start-up) data sets were provided for these time-shift calculation tests. Previous work from others has seen a low magnitude of time-shifts (around 1 ms) in this period (Falahat 2012). These time-shifts were estimated either by subtracting time differences of interpreted horizons or by modelling the effect of pressure and saturation changes, respectively. An NRMS map was generated for an interval of 300–600 ms above the reservoir, using equations proposed by Kragh and Christie (2002), showing the poor repeatability in seismic data sets (Fig. 15).

Time-lapse map of the sum of negative amplitude between the top and base reservoir was generated in Fig. 16. Instantaneous time-shift maps were extracted at the base reservoir (Fig. 17). Despite the high noise level, they show similar character of positive time-shift distribution, as indicated. The distribution also correlates with the softening signals shown in the RMS amplitude map in some areas.

The three time-shift sections displayed in Fig. 17 are extracted from line AA′. All manage to show extension signals in the under-burden that are mainly due to geomechanical effects. Central overburden extension is observed in all three results, but the positive time-shift on the left side caused by a producing well is lost in the DHFCC result. In terms of noise level, NLI behaves much better than the DHFCC and CLM methods.

4.4 Discussion of the Best Method

The time-shift and time-strain results from the previous analysis are all summarized in Figs. 18, 19, and 20. A marking scheme is introduced here to compare the efficiency of the three time-shift measurement techniques. Scores of between 0 and 10 are given for each field application, to account for aspects such as result noise, resolution, and time-strain quality. High marks are given to low values of the first two aspects, but high values of the last two aspects.

In terms of time-shift quality, taking Erskine as an example, DHFCC generates the worst result among the three, so it is assigned a score of 6 (3 for resolution and 3 for noise level). NLI suppressed noise better than CLM in the western part, whereas the pattern of the CLM time-shift map coincides well with the distribution of the two main faults, so NLI scores 15 (5 for resolution and 10 for noise level), and CLM scores 16 (9 for resolution and 7 for noise level).

In terms of time-strain quality, taking the Ekofisk towed streamer results, for example, they all show relatively good resolution, as they reveal the strong compaction signal inside the reservoir and extension signals above the top reservoir and under the base reservoir. Because of the nature of the derivation process, all the time-strain results have high noise levels, but DHFCC and NLI are better than CLM, as they already involve smoothing techniques when generating time-shifts. Therefore, in this aspect, scores of 7, 9, and 5 are allocated to DHFCC, NLI, and CLM, respectively.

In terms of the computational cost, under the current conditions of our research team's cluster and when dealing with seismic data sets less than 1 gigabyte, it takes about 1 h for DHFCC, 6 h for CLM, and 4 h for NLI. Of course, time will be reduced with a smaller seismic data set and a more powerful cluster as well; therefore, this will not be included in our marking criteria.

Finally, after summing all the marks in each aspect, NLI is regarded as the best method for this research, as it generates both good time-shifts and stable time strains. The marking detail is shown in Table 2. For generating better maps, this technique needs to be extended from two dimensions to three dimensions. The traditional cross-correlation-based method is still good for time-shift calculation in many cases. In terms of good resolution, CLM is the best. However, as none of those smoothing techniques are imposed, further tricks for suppressing noise are needed to make it a robust technique.

Table 2 Marks for each method, based on time-shift and time-strain quality

Fields	Methods	Time-shift quality		Time-strain quality (0–10)	Total mark (0–30)
		Noise level (0–10)	Resolution (0–10)		
Ekofisk (03-89)	DHFCC	8	6	7	21
	CLM	6	8	5	19
	NLI	9	6	9	24
Ekofisk (LoFS2-1)	DHFCC	6	6	5	15
	CLM	4	7	4	15
	NLI	7	6	6	19
Erskine (01-89)	DHFCC	3	3	3	9
	CLM	7	9	3	19
	NLI	10	5	4	19
Schiehallion (02-96)	DHFCC	8	5	5	18
	CLM	6	6	7	19
	NLI	9	5	6	20

5 Conclusions

This paper has provided a critical review of three typical time-shift calculation methods.

With application to a set of synthetic tests which were designed to evaluate the accuracy in recovering various time-shifts, it was found that in the case of large time-shifts, the DHFCC method did a very good job in recovering a stable time-shift profile, even when dealing with very noisy seismic data. However, the accuracy of the CLM and NLI methods decreased with the increase in the noise level in seismic data. In the case of recovering small time-shifts, despite still giving a stable result, DHFCC lost its accuracy, while NLI and CLM tended to give better results.

The three time-shift measurement techniques were then applied to four North Sea data sets, among which the seismic quality and time-shift magnitude varied. A marking scheme was established for method comparison in terms of computational cost, and time-shift and time-strain quality. NLI was found to be the best method for this research, as it generates both good time-shifts and stable time strains. The resolution of the DHFCC method and the noise suppression ability of the CLM method need to be improved if they are to be considered for future use.

References

Behrens R, Condon P, Haworth W, et al (2001) 4D seismic monitoring of water influx at Bay Marchand: the practical use of 4D in an imperfect world. In: 2001 SPE annual technical conference and exhibition. New Orleans, Louisiana, p SPE 71329

Buizard S, Bertrand A, Nielsen KM, et al (2013) Ekofisk life of field seismic: 4D processing. In: 75th EAGE conference & exhibition incorporating SPE EUROPEC 2013, London, UK

Falahat R (2012) Quantitative monitoring of gas injection, exsolution and dissolution using 4D seismic. Heriot-Watt University, Edinburgh

Fehmers GC, Hunt K, Brain JP, et al (2007) Curlew D: pushing the boundaries of 4D depletion signal in a gas condensate field, UK Central North Sea. In: EAGE 69th conference & exhibition. London, UK, p P074

Fletcher J (2004) Rock and fluid physics understanding the impact of pressure changes: what do petroleum engineers expect from time lapse seismic, and do geophysicists answer the right questions? In: SPE/EAGE Joint Workshop, Copenhagen, Denmark, 23–25 March 2004

Folstad PG (2010) Monitoring of the Ekofisk field. Geo ExPro 7:72–76

Fuck RF, Bakulin A, Tsvankin I (2007) Time-lapse traveltime shifts above compacting reservoirs: 3D solutions for prestack data. In: SEG 2007 annual meeting. San Antonio

Grandi A, Wauquier S, Cumming H et al (2009) Quantitative 4D time lapse characterisation: three examples. In: SEG Houston 2009 international exposition and annual meeting, Houston, USA, pp 3815–3819. https://doi.org/10.1190/1.3255662

Gubbins D (2004) Time series analysis and inverse theory for geophysicists. Cambridge University Press, Cambridge

Hajnasser Y (2012) The implications of shale geomechanics and pressure diffusion for 4D interpretation. Ph.D. thesis, Heriot-Watt University, UK

Hale D (2007) A method for estimating apparent displacement vectors from time-lapse seismic images. In: SEG/San Antonio 2007 annual meeting. pp 2939–2943

Hale D (2009) A method for estimating apparent displacement vectors from time-lapse seismic images. Geophysics 74(5):V99

Hall SA, MacBeth CA, Barkved OI, Wild P (2002) Time-lapse seismic monitoring of compaction and subsidence at Valhall through crossmatching and interpreted warping of 3D streamer and OBC data. In: 72nd SEG annual international meeting. Salt Lake City, Utah, pp 1696–1699

Hatchell P, Bourne S (2005) Rocks under strain: strain-induced time-lapse time shifts are observed for depleting reservoirs. Lead Edge 24:1222–1225

Hatchell P, Van Den Beukel A, Molenaar M et al (2003) Whole earth 4D: reservoir monitoring geomechanics. In: 73rd SEG meeting, Dallas, USA. https://doi.org/10.1190/1.1817532

Hodgson N (2009) Inversion for reservoir pressure change using overburden strain measurements determined from 4D seismic. Ph.D. thesis, Heriot-Watt University, UK

Kanu C, Toomey A, Hodgson L et al (2016) Evaluation of time-shift extraction methods on a synthetic model with 4D geomechanical changes. Leading Edge 35:888–893. https://doi.org/10.1190/tle35100888.1

Kloosterman HJ, Kelly RS, Stammeijer J et al (2003) Successful application of time-lapse seismic data in shell expro's gannet fields, Central North Sea, UKCS. Pet Geosci 9:25–34. https://doi.org/10.1144/1354-079302-513

Koster K, Gabriels P, Hartung M et al (2000) Time-lapse seismic surveys in the North Sea and their business impact. Leading Edge 19:286–293. https://doi.org/10.1190/1.1438594

Kragh E, Christie P (2002) Seismic repeatability, normalized RMS, and predictability. Lead Edge 21:640–647

Kvendseth SS (1988) Giant discovery: a history of ekofisk through the first 20 years. Phillips Petroleum Company Norway

Landrø M (2001) Discrimination between pressure and fluid saturation changes from marine multicomponent time-lapse seismic data. Geophysics 66:836–844. https://doi.org/10.1190/1.1620633

Landrø M, Janssen R (2002) Estimating compaction and velocity changes from time-lapse near and far offset stacks. In 64th EAGE conference & exhibition. Florence, Italy, p P036

Landrø M, Stammeijer J (2004) Quantitative estimation of compaction and velocity changes using 4D impedance and traveltime changes. Geophysics 69(4):949–957

Lie EO (2011) Constrained timeshift estimation. In: 73rd EAGE conference & exhibition incorporating SPE EUROPEC 2011. Vienna, Austria, p G038

MacBeth C, Mangriotis M, Hatchell P (2016) Evaluation of the spurious time-shift problem. In: SEG International exposition and 86th annual meeting. P 5457-5462

MacBeth C, Mangriotis MD, Amini H (2019) Post-stack 4D seismic time-shifts: Interpretation and evaluation. Geophys Prospect 67:3–31. https://doi.org/10.1111/1365-2478.12688

Martin K, Macdonald C (2010) The Schiehallion field : applying a geobody modelling approach to piece together a complex turbidite field. In: 7th European production and development conference, Aberdeen, UK

Nickel M, Schlaf J, Sonneland L (2001) New tools for 4D seismic analysis in carbonate reservoirs. In: SEG exposition and annual meeting, San Antonio, Texas

Rickett J, Duranti L, Hudson T, et al (2006) Compaction and 4-D time strain at the Genesis Field. In: SEG/New Orleans 2006 annual meeting, 2006, New Orleans, USA, pp 3215–3219

Rickett J, Duranti L, Hudson T et al (2007) 4D time strain and the seismic signature of geomechanical compaction at Genesis. Lead Edge 26:644. https://doi.org/10.1190/1.2737103

Sulak RM, Danielsen J (1989) Reservoir aspects of Ekofisk subsidence. J Pet Technol 41:709–716. https://doi.org/10.2118/17852-pa

Tolstukhin E, Lyngnes B, Sudan H. (2012) Ekofisk 4D seismic: seismic history matching workflow. In: EAGE annual conference & exhibition incorporating SPE Europec, Copenhagen, Denmark, pp 4–7

Whitcombe DN, Paramo P, Philip N, et al (2010) The correlated leakage method: it's application to better quantify timing shifts on 4D data. In: 72nd EAGE conference & exhibition incorporating SPE EUROPEC 2010, p B037

Williamson P, Cherrett A, Sexton P (2007) A new approach to warping for quantitative time–lapse characterisation. In: 69th EAGE conference & exhibition, London, UK

Wong M (2017) Pressure and saturation estimation from PRM timelapse seismic data for a compacting reservoir. Ph.D. thesis, Heriot-Watt University, UK

Zabihi Naeini E (2013) TT domain time shift estimation. In: 75th EAGE conference & exhibition incorporating SPE EUROPEC 2013, pp 10–13